

## **Process Mapping for Qualification Across Multiple Direct Metal Additive Manufacturing Processes**

Jack Beuth, Jason Fox, Joy Gockel, Colt Montgomery, Rui Yang, Haipeng Qiao, Emrecan Soylemez, Pete Reeseewatt, Amin Anvari, Sneha Narra and Nathan Klingbeil\*

Department of Mechanical Engineering, Carnegie Mellon Univ., Pittsburgh, PA 15213

\*Department of Mechanical & Materials Engineering, Wright State Univ., Dayton, OH, 45435

### **Abstract**

This paper gives an overview of work by the authors developing process mapping methods for additive manufacturing (AM), capturing the dependence of melt pool geometry and microstructure on primary processing variables under steady-state and transient conditions. This work is being applied to the task of process qualification and is being applied across multiple AM processes including electron beam wire feed, electron beam powder bed, laser powder bed, and laser powder stream processes. Process mapping methods are now allowing all of these processes acting in very different regions of processing space to be characterized and analyzed in a unified way. A few insights from this approach are summarized.

### **Introduction**

Additive Manufacturing (AM) currently encompasses a wide range of technologies meant to transform CAD models of components into 3-D prototypes or final production parts. Processes range from low-cost machines targeting the consumer market (e.g. Makerbot<sup>®</sup> or Cube<sup>®</sup> systems) to industrial polymer systems (e.g. FDM by Stratasys) to high-end direct metal systems (e.g. Arcam EBM<sup>®</sup> and Sciaky Direct Manufacturing). Recently, significant excitement has been generated by the fully automated building of 3-D shapes out of metals by commercial laser and electron beam powder bed direct metal AM systems.

Despite the substantial recent advances in AM technologies across the cost spectrum, it is true that almost all of these advances have come from extensive experimentation coupled with intuition. For the direct metal processes, development of process variable sets by machine manufacturers for the fabrication of shapes of a single alloy system is time and cost intensive. There is limited knowledge of how to transfer processing knowledge across metal alloy systems and across different direct metal processes. There is also limited understanding of how to alter process variables outside of established process variable sets for a single machine and alloy system.

This paper outlines work by the authors developing process mapping methods for AM, designed to address the problems noted above by capturing the dependence of process characteristics (e.g. melt pool geometry, microstructure and residual stress) on primary processing variables under steady-state and transient conditions. The methods are entirely general, and are applicable to all thermally-based AM processes; however, focus will be directed in this paper on direct metal AM systems.

Beuth and collaborators have pursued various forms of thermal modeling and process mapping research for more than 15 years. The term “process mapping” applied to AM was originated by the authors to denote mapping of process outcomes in terms of process variables. Early work addressed the modeling and measurement of residual stress in metal and polymer deposition SFF processes [1-4]. Control of melt pool size under steady-state conditions for laser-based SFF processes has been considered by plotting nondimensional melt pool size metrics over the full range of process variables for LENS<sup>®</sup> [5-8]. The process map approach has been extended to consider melt pool size control under transient conditions and as a function of process size scale [9-12]. In the work on transient melt pool response, numerically determined melt pool response times are used to establish a lower bound on the response times of thermal feedback control systems for LENS<sup>®</sup>. In the work on process size scale, the role of process size on the sensitivity of melt pool size to fluctuations in beam power or velocity are related to process robustness. The issue of residual stress control for laser-based SFF has also been addressed using a process map approach [13, 14]. In that work, a defined thermal gradient behind the melt pool is proposed as a means for predicting changes in final magnitudes of residual stress based on thermal simulation results. The work of [15] applies this approach to the concept of stress reduction by localized part preheating via a dual-beam laser or electron beam system. A combined modeling and experimental study of melt pool dimensional control for wire feed electron beam processes is presented in [16].

While the work outlined above has been centered at Carnegie Mellon, thermal modeling has also been pursued at Wright State related to microstructure control in AM processes. Analytical calculations and finite element simulations have been used by Klingbeil and co-authors to observe cooling rates and thermal gradients and their relation to grain morphology in beam-based manufacturing [17-20]. A study of process variable (beam power and velocity) effects has shown that microstructure can vary significantly throughout the depth of the deposit, and that under high power conditions a transition from columnar to mixed columnar and equiaxed structures is possible [21]. The effect of free-edges on melt pool geometry and solidification microstructure has also been considered [22-24].

The primary approach applied at Wright State to prediction and control of microstructure (grain size and morphology) in beam-based additive manufacturing processes [17-22] is based on the development of maps for solidification cooling rate and thermal gradient (the key parameters controlling solidification microstructure) in conjunction with solidification maps for Ti64. The expected grain morphology can be predicted as either equiaxed, columnar or mixed by plotting points numerical results for cooling rates and thermal gradients on the “solidification map”, which has been previously calibrated for Ti64 [26].

The process mapping research outlined above has involved the mapping of specific numerical results for single processes, usually in terms of nondimensional quantities. While offering intuition, its format was not broadly applicable or easily useable in industrial settings. Most recently, work at Carnegie Mellon and Wright State has yielded patent pending process mapping approaches that are not only directly useable in industrial applications, but are entirely general, useable in mapping either numerical or experimental results and applicable to the building of generic 3-D shapes by any thermally-based AM or related process. This paper outlines some of the applications of these latest approaches.

## The Process Map Approach

As embodied in multiple patent filings [27,28,30,31,33], the process map approach as applied to AM identifies five primary process variables of importance in any thermally-based AM process. They are heat source power ( $P$ ), heat source travel speed (velocity,  $V$ ), material feed rate (MFR or other variable defining MFR), existing temperature of the part or component being deposited onto ( $T_0$ ) and feature geometry (the local geometry of the part). While it is recognized that, depending on the process, other process variables (such as average powder particle size or beam spot size) may affect process outcomes, the approach involves mapping AM processes in terms of the five primary process variables first. Once that behavior is mapped, if needed, a detailed study of the role of a secondary process variable can be carried out to evaluate its effects on the process across the full five-primary-variable processing space.

Although process mapping can be represented in many ways, a format most amenable to AM developers and users is a P-V process map, where results are presented on a two-dimensional plot of power (y axis) vs. velocity (x axis) for a single value of MFR,  $T_0$  and for a single feature geometry. Figure 1 shows three example feature geometries (or geometric primitives) that can be mapped, due to their importance in building up 3-D shapes. In each case, the shaded bead is the one currently being deposited. The single bead geometry (single bead in the middle of a part, away from the free edges) is the simplest of the three. The successive bead geometry is applicable to raster type patterns where a beads are deposited next to each other. Unlike the first two geometries, the third geometry (deposition along an external radius) is a transient geometry where thermal conditions are also a function of location along the bead path. Details of how these geometries can effectively be mapped and compared are given in [27,28].

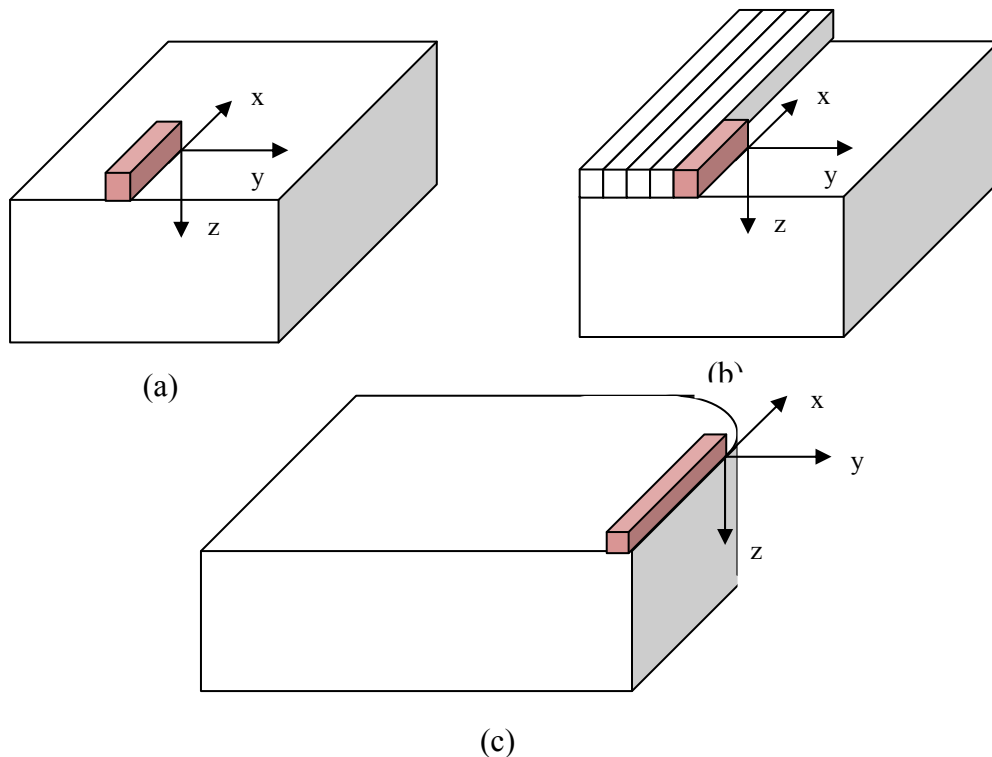


Figure 1: Example feature or primitive geometries that can be process mapped: a) single bead b) successive bead and c) external radius geometries

The authors and collaborators are currently applying this approach to “map out” the major types of currently available commercial direct metal AM processes. These include laser powder stream (LENS<sup>®</sup>), laser powder bed (Direct Metal Laser Sintering by EOS), electron beam powder bed (EBM<sup>®</sup> by Arcam) and electron beam wire feed (Direct Manufacturing by Sciaky). Process outcomes being mapped include melt pool size and shape and a variety of microstructural features. This mapping is being performed based on both numerical model and experimental results, developing methods for performing minimum numbers of experiments to fully map out process behavior. All process maps presented in this paper are derived from finite element simulations.

### **A P-V Map for Melt Pool Geometry for Ti64 and Wire Feed Electron Beam AM**

As an example of a P-V process map, Figure 2 provides a process map for controlling melt pool geometry in wire feed e-beam AM processes for a single bead geometry (Fig 1a), with a value of  $T_0 = 303\text{K}$  and a fixed ratio of deposited material to total melted material of  $\phi = 0.77$ . Note that in using the P-V map,  $\phi$  is maintained as a constant as  $V$  is changed if the material feed rate (the wire feed rate) is changed proportionally with  $V$ . Plotted in green, red and blue are curves of constant maximum melt pool cross sectional area,  $A$ , as a function of absorbed beam power and beam velocity. Here the cross section is normal to the direction of beam travel, so that  $A$  is directly related to bead cross sectional area - a critical dimension to control in building shapes. Plotted in lavender, turquoise and orange are curves of constant  $L/d$  ratio, where  $d$  is the maximum effective melt pool depth (defined as  $d = \sqrt{2A/\pi}$ ) and  $L$  is the melt pool length from the point of maximum depth to the melt pool trailing edge. Together, the curves of constant  $A$  and  $L/d$  in Fig. 2 map out melt pool size ( $A$ ) and shape ( $L/d$ ) control for single bead deposits over the full range of beam powers in medium-scale wire feed electron beam AM processes.

The plot of Fig. 2 can be used as a guide for selecting wide ranges of values of beam power, beam velocity and material feed rate to yield a constant  $A$  or  $L/d$ . This allows processing researchers to switch from high powers, high velocities and high deposition rates for reduced build time to low powers, low velocities and low deposition rates for increased precision in how material is deposited.

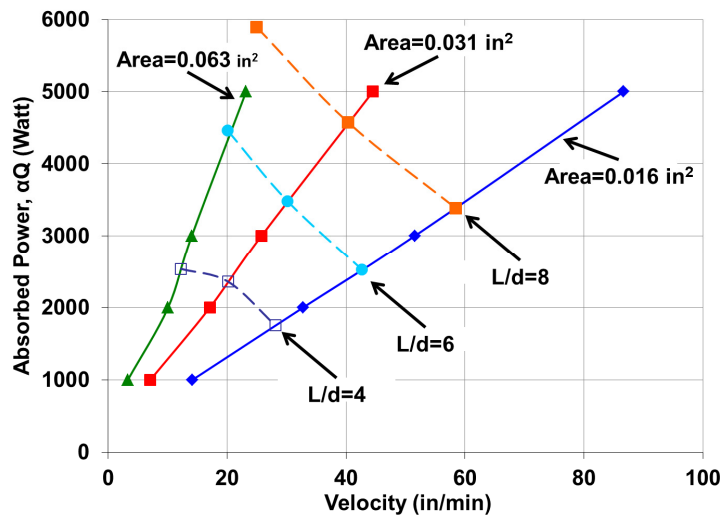


Figure 2: Process map for controlling melt pool dimensions for single bead Ti64 deposition in wire feed e-beam AM

## Other Geometries

The geometry of a single bead in the middle of a plate is the simplest of those of interest in AM. As outlined in [27,28] there are a variety of elementary geometries that be mapped that, once completed, can be combined to allow a general 3-D shape of a given material to be fabricated. Another simple geometry is that of single bead deposition along a free edge. A separate diagram for this geometry is not provided in Fig. 1, but it would correspond to the geometry of Fig. 1c for the case of a deposition location that is far away from the external radius (either well before or well after the radius is encountered). Fig. 3 provides a P-V process map for maximum effective melt pool depth and  $L/d$  for this case, again for a wire-feed e-beam AM process. In Fig. 3, the effective melt pool depths have been chosen to correspond to the same melt pool areas as plotted in Fig. 2, so a direct comparison can be made between green, red and blue curves of constant  $A$  or  $d$  in the two plots.

Figure 3 demonstrates that with respect to melt pool area or effective melt pool depth, the effect of changing from single bead deposited in the middle of a part to one deposited at a free edge simply causes the  $A$  and  $L/d$  curves to rotate and shift. For the free edge case, this results in lower power and/or higher velocity needed to yield the same  $A$  or  $d$  as for the case of the bead in the middle of the plate. This is due to the reduced path for conduction into the substrate for the free edge case. Changes in the  $L/d$  curves are more severe, with the shape of the curves changing and with substantial shifts toward higher  $P$  and  $V$  values in the free edge case.

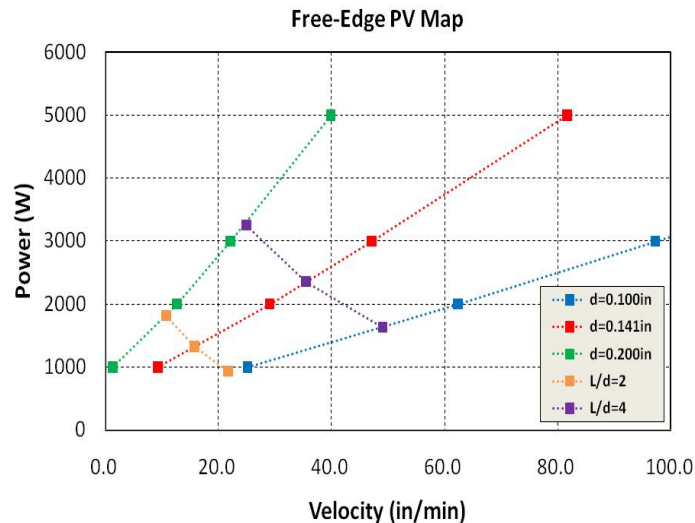


Figure 3. Process map for deposition along a free edge

To gain further insight, transitions between the cases mapped in Fig. 2 and Fig. 3 can be considered. Figure 4 provides a plot of three curves for  $d$  at three fixed  $P, V$  combinations, as a function of distance from the free edge. Thus the right side of the plot corresponds to the cases mapped in Fig. 2. The left edge of the plot corresponds to the cases mapped in Fig. 3. For each of the 3 curves, the fixed  $P, V$  combinations are taken from locations on the single bead (Fig. 2) blue line. What is seen is that the curves essentially lie on top of one another, demonstrating that cases with the same melt pool depth in the single bead case will have essentially the same increases in melt pool depth as a function of distance from a free edge. Further, the distance

from the free edge at which the free edge effects are first seen is consistent and approximately 2 melt pool depths. In this way, the process mapping approach has yielded insights that can significantly decrease the complexity of understanding AM process control.

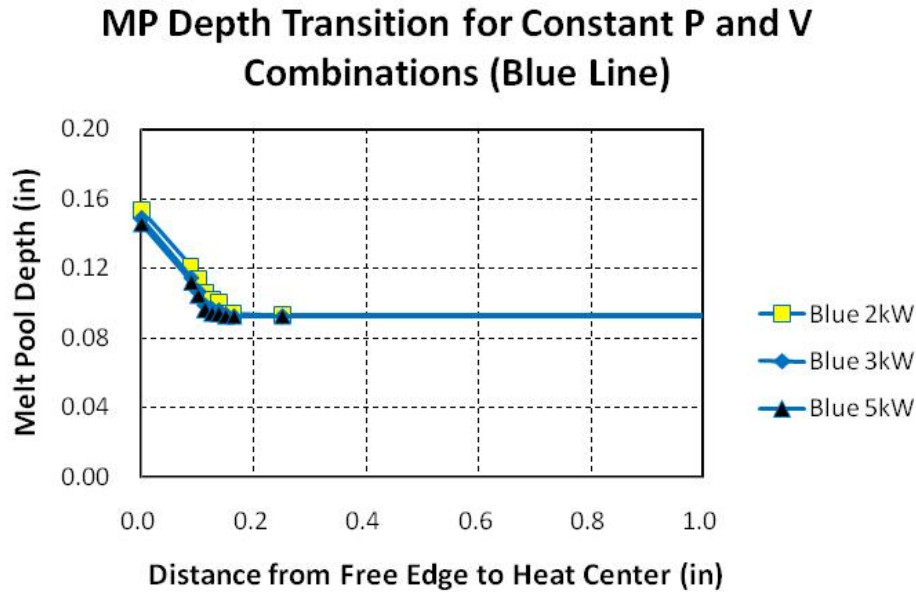


Figure 4. Melt pool depth as a function of distance from the free edge for fixed P, V

### Other Processes

The currently available commercial direct metal AM processes were largely developed independently of one another and span a wide range of process variables. Even the two major classes of powder bed direct metal processes (laser-based and electron beam-based) operate in very different regions of process variable space. Figure 5 illustrates this with approximate P,V operating ranges of four commercial direct metal AM processes. The figure is approximate in that it does not identify machine limits (which can be much larger than what is indicated in the figure), but approximate maximum ranges used in part fabrication. Also, with respect to practical operating ranges, the limits used in the plot are somewhat liberal. In practice the actual ranges of P and V used to fabricate a single part may be much smaller. It should also be noted that there are now a number of laser powder bed processes competing with EOS, operating in roughly the same region of P-V space, however, there are some differences in available laser powers. Also, the Sciaky process operating range can extend to significantly higher powers in some models (to 10kW and higher).

Results presented thus far have been for a small to medium sized wire feed e-beam process (e.g. Sciaky) designated in the upper left corner of the plot. However, process mapping methods can just as easily be applied to any region in the P-V space shown in Fig. 5. This is illustrated by Fig. 6, which shows a P-V process map for A and L/d for Ti64 single bead deposition via the Arcam EBM<sup>®</sup> process. The first thing to note from the figure is that other than the very different P and V scale values, the curves look very similar to those for Ti64 deposition

by wire feed e-beam AM. Clearly the melt pool area values are much smaller and the L/d values are much larger for EBM<sup>®</sup>. Interspersed with the curves are experimental values of melt pool areas (from experiments performed by Ola Harrysson's group at North Carolina State University), plotted under the assumption that 90% of the e-beam power at the source is absorbed into the substrate. Although these are from a first set of EBM<sup>®</sup> tests, and more analysis and testing are needed, it is clear that the measured melt pool cross sectional areas are largely consistent with the numerical model predictions.

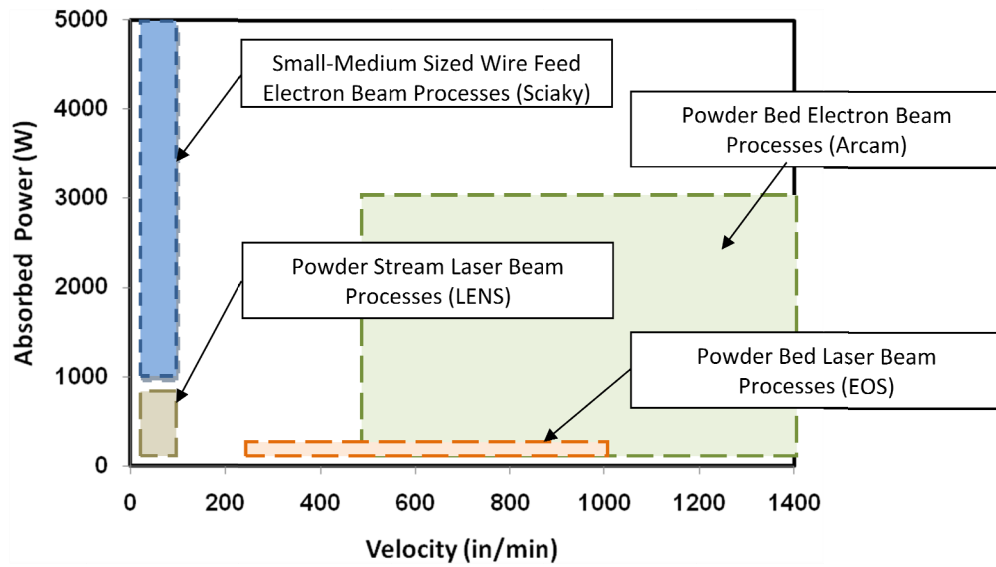


Figure 5 Approximate regions of P-V space occupied by currently available commercial direct metal AM processes

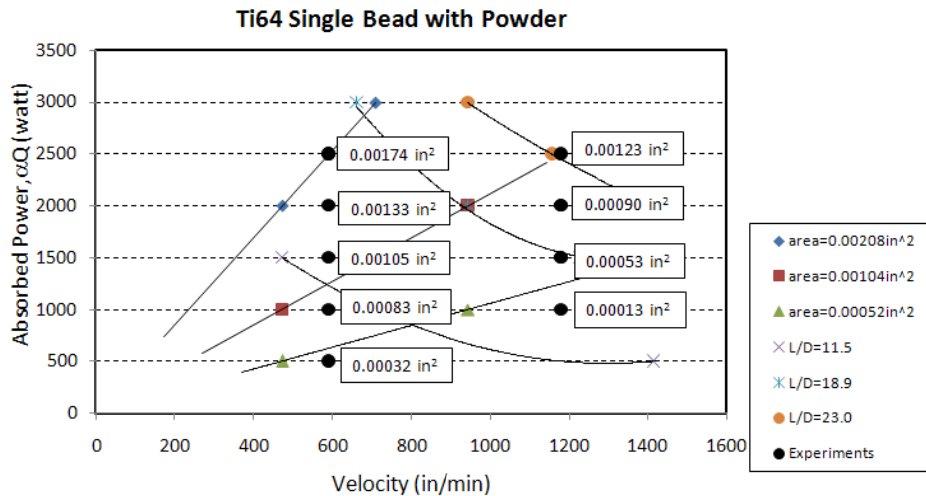


Figure 5 P-V Map for single bead deposition for the Arcam EBM<sup>®</sup> process

## Other Alloys

Sets of process maps can be developed for multiple alloy systems, yielding the ability to compare directly the process variable dependence of key process outcomes between alloys. This is illustrated in Fig. 6 with a P-V process map of constant melt pool area curves for CoCr and IN625 alloys for a single bead geometry. In this case, the range of P and V are consistent with the EOS Direct Metal Laser Sintering process. Again, it is clear that the constant area curves in Fig. 6 are qualitatively similar to those in Figs 2, 3 and 5. The plot of Fig. 6 also suggests that due to the uncomplicated changes in the curves in switching from one alloy system to another, process maps have the potential for greatly simplifying the development of process variable sets for new alloy systems.

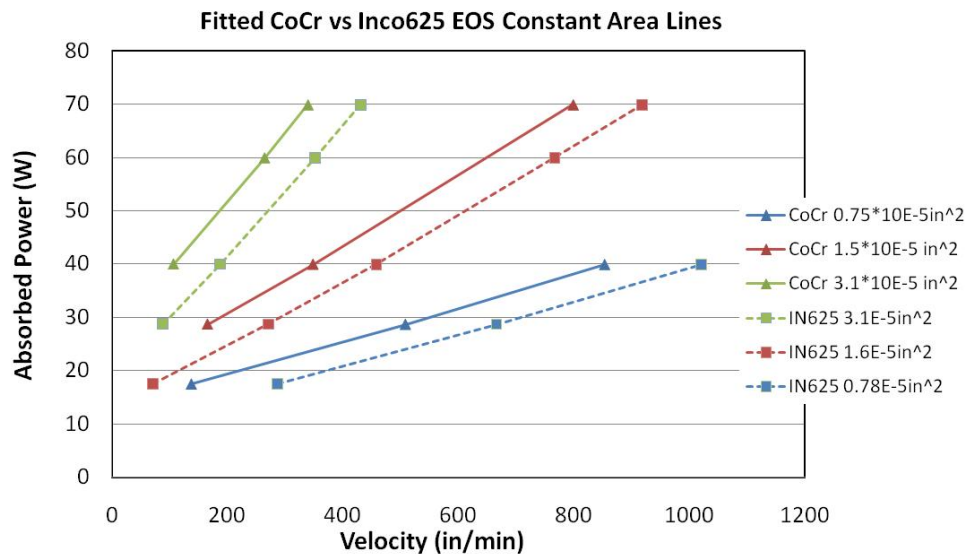


Figure 6 P-V Map for single bead deposition for the EOS Direct Metal Laser Sintering process for CoCr and IN 625 alloys

## Other Applications

In two other papers in this symposium proceedings, two additional applications of process mapping are explored. In the paper by Gockel and Beuth [29], process mapping of microstructural features is considered, following methods outlined in the patent applications [30,31]. That work demonstrates that not only can microstructure be process mapped, but that comparisons between process maps for melt pool dimensions and microstructure can yield approaches for the indirect real-time control of microstructure through the direct real time control (via a thermal imaging system, for instance) of melt pool dimensions.

In the paper by Fox and Beuth [32] process mapping of the transient response of melt pool geometry is considered, following methods outlined in the patent application [33]. That work demonstrates how to map melt pool response times due to abrupt changes in beam powers and travel speeds, with application to real time melt pool feedback control systems. That work

demonstrates that melt pool response times can be long, and that the process mapping approach can yield insights into the physics that greatly simplify understanding of the dependence of response time on process variables.

### **Conclusions**

This paper has outlined some aspects of a process mapping approach for AM. These include the effects on melt pool geometry of changes in feature geometry, process, and alloy system being considered. The approach is also applicable to the mapping of microstructural features and melt pool transient response across processing space. The approach can be applied across all direct metal AM processes and can be applied to other thermally-based AM processes (for polymers, for instance). The authors are currently process mapping the major classes of direct metal AM processes via numerical modeling and experimentation.

### **Acknowledgements**

The authors wish to acknowledge collaborations with Ola Harrysson of North Carolina State University and his research group and for Arcam EBM<sup>®</sup> experiments performed at NC State for this research. This research was supported by the National Science Foundation under grant CMMI-1131579 and by the National Institute of Standards and Technology under grant 70NANB12H263.

### **References**

1. Klingbeil, N.W., Zinn, J.W. and Beuth, J.L., "Measurement of Residual Stresses in Parts Created by Shape Deposition Manufacturing," *Solid Freeform Fabrication Proceedings*, Proc. 1997 Solid Freeform Fabrication Symposium, Austin, August 1997, pp. 125-132.
2. Klingbeil, N.W., Beuth, J.L., Chin, R.K., and Amon, C.H., "Measurement and Modeling of Residual Stress-Induced Warping in Direct Metal Deposition Processes," *Solid Freeform Fabrication Proceedings*, Proc. 1998 Solid Freeform Fabrication Symposium, Austin, August 1998, pp. 367-374.
3. Ong, R., Beuth, J.L. and Weiss, L.E., "Residual Stress Control Issues for Thermal Deposition of Polymers in SFF Processes," *Solid Freeform Fabrication Proceedings*, Proc. 2000 Solid Freeform Fabrication Symposium, Austin, August 2000, pp. 209-218.
4. Klingbeil, N.W., Beuth, J.L., Chin, R.K. and Amon, C.H., "Residual Stress-Induced Warping in Direct Metal Solid Freeform Fabrication," *International Journal of Mechanical Sciences*, Vol. 44, 2002, pp. 57-77.
5. Vasinonta, A., Beuth, J.L. and Griffith, M.L., "Process Maps for Laser Deposition of Thin-Walled Structures," *Solid Freeform Fabrication Proceedings*, Proc. 1999 Solid Freeform Fabrication Symposium, Austin, August 1999, pp. 383-391.
6. Vasinonta, A., Beuth, J.L., and Ong, R., "Melt Pool Size Control in Thin-Walled and Bulky Parts via Process Maps," *Solid Freeform Fabrication Proceedings*, Proc. 2001 Solid Freeform Fabrication Symposium, Austin, August 2001, pp. 432-440.
7. Vasinonta, A., Beuth, J.L. and Griffith, M.L., "A Process Map for Consistent Build Conditions in the Solid Freeform Fabrication of Thin-Walled Structures," *Journal of Manufacturing Science and Engineering*, Vol. 123, No. 4, 2001, pp. 615-622.

8. Beuth, J.L. and Klingbeil, N.W., "The Role of Process Variables in Laser-Based Direct Metal Solid Freeform Fabrication," *JOM*, September 2001, pp. 36-39.
9. Aggarangsi, P., Beuth, J.L., and Griffith, M.L., "Melt Pool Size and Stress Control for Laser-Based Deposition Near a Free Edge," *Solid Freeform Fabrication Proceedings*, Proc. 2003 Solid Freeform Fabrication Symposium, Austin, August 2003, pp. 196-207.
10. Birnbaum, A.J., Aggarangsi, P. and Beuth, J.L., "Process Scaling and Transient Melt Pool Size Control in Laser-Based Additive Manufacturing Processes," *Solid Freeform Fabrication Proceedings*, Proc. 2003 Solid Freeform Fabrication Symposium, Austin, August 2003, pp. 328-339.
11. Aggarangsi, P., Beuth, J.L., and Gill, D.D., "Transient Changes in Melt Pool Size in Laser Additive Manufacturing Processes," *Solid Freeform Fabrication Proceedings*, Proc. 2004 Solid Freeform Fabrication Symposium, Austin, August 2004, pp. 163-174.
12. Birnbaum, A.J., Beuth, J.L. and Sears, J.W., "Scaling Effects in Laser-Based Additive Manufacturing Processes," *Solid Freeform Fabrication Proceedings*, Proc. 2004 Solid Freeform Fabrication Symposium, Austin, August 2004, pp. 151-162.
13. Vasinonta, A., Beuth, J.L. and Griffith, M.L., "Process Maps for Controlling Residual Stress and Melt Pool Size in Laser-Based SFF Processes," *Solid Freeform Fabrication Proceedings*, Proc. 2000 Solid Freeform Fabrication Symposium, Austin, August 2000, pp. 200-208.
14. Vasinonta, A., Beuth, J.L., and Griffith, M.L. "Process Maps for Predicting Residual Stress and Melt Pool Size in the Laser-Based Fabrication of Thin-Walled Structures," *ASME Journal of Manufacturing Science and Engineering*, Vol. 129, No. 1, 2007, pp. 101-109.
15. Aggarangsi, P and Beuth, J.L., "Localized Preheating Approaches for Reducing Residual Stress in Additive Manufacturing," *Solid Freeform Fabrication Proceedings*, Proc. 2006 Solid Freeform Fabrication Symposium, Austin, August 2006, pp. 709-720.
16. Soylemez, E., Beuth, J.L. and Taminger, K., "Controlling Melt Pool Dimensions over a Wide Range of Material Deposition Rates in Electron Beam Additive Manufacturing," *Solid Freeform Fabrication Proceedings*, Proc. 2010 Solid Freeform Fabrication Symposium, Austin, August 2010.
17. Bontha, S. and Klingbeil, N., "Thermal Process Maps for Controlling Microstructure in Laser-Based Solid Freeform Fabrication," in *Solid Freeform Fabrication Proceedings*, Proc. 2003 Solid Freeform Fabrication Symposium, Austin, August 2003, pp. 219-226.
18. Klingbeil, N., Bontha, S., Brown, C., Gaddam, D., Kobryn, P., Fraser, H., and Sears, J., "Effects of Process Variables and Size Scale on Solidification Microstructure in Laser - Based Solid Freeform Fabrication of Ti-6Al-4V," *Solid Freeform Fabrication Proceedings*, Proc. 2004 Solid Freeform Fabrication Symposium, Austin, August 2004.
19. Bontha, S., Klingbeil, N., Kobryn, P., and Fraser, H., "Thermal Process Maps for Predicting Solidification Microstructure in Laser Fabrication of Thin Wall Structures," *Journal of Materials Processing Technology*, vol. 178, no. 1-3, pp. 135-142, 2006.
20. Bontha, S., "The Effect of Process Variables on Microstructure in Laser-Deposited Materials," Ph.D. Thesis, Wright State University, June 2006.
21. Bontha, S., Klingbeil, N. W., Kobryn, P.A. and Fraser, H. L., "Effects of Process Variables and Size-Scale on Solidification Microstructure in Beam-Based Fabrication of Bulky 3D Structures," *Materials Science and Engineering A*, Vol. 513-514, 2009, pp. 311-318.
22. Davis, J., Klingbeil, N., and Bontha, S., "Effect of Free-Edges on Melt Pool Geometry and Solidification Microstructure in Beam-Based Fabrication of Thin-Wall Structures," *Solid*

- Freeform Fabrication Proceedings*, Proc. 2009 Solid Freeform Fabrication Symposium, Austin, August 2009.
23. Davis, J., Klingbeil, N., and Bontha, S., "Effect of Free-Edges on Melt Pool Geometry and Solidification Microstructure in Beam-Based Fabrication of Bulky 3-D Structures," *Solid Freeform Fabrication Proceedings*, Proc. 2010 Solid Freeform Fabrication Symposium, Austin, August 2010.
  24. Davis, J.E., "Effect of Free-Edges on Melt Pool Geometry and Solidification Microstructure in Beam-Based Fabrication Methods," Master's thesis, Wright State University, 2010.
  25. Wang, L., Felicelli, S. D., and Craig, J.E., "Experimental and Numerical Study of the LENS Rapid Fabrication Process," *Journal of Manufacturing Science and Engineering*, Vol. 131, No. 4, 2009, pp. 041019.1-041019.8.
  26. Kobryn, P. and Semiatin, S., "Microstructure and Texture Evolution during Solidification Processing of Ti-6Al-4V," *Journal of Materials Processing Technology*, vol. 135, pp. 330–339, 2003.
  27. Beuth, J.L., Methods for Determining Process Variable Combinations Yielding Constant Melt Pool Geometry for Single Bead Deposits in Direct Digital Manufacturing, 61/574,253, filed July 29, 2011.
  28. Beuth, J.L., "Process Mapping of Melt Pool Geometry," PCT/US2012/048658, filed July 27, 2012.
  29. Gockel, J.D. and Beuth, J.L., "Understanding Ti-6Al-4V Microstructure Control in Additive Manufacturing via Process Maps," *Solid Freeform Fabrication Proceedings*, Austin, August 2013 (in the current proceedings).
  30. Beuth, J.L., Klingbeil, N.W. and Gockel, J.D., "Process Mapping of Cooling Rates and Thermal Gradients," 61/742,734, filed August 17, 2012.
  31. Beuth, J.L., Klingbeil, N.W. and Gockel, J.D., "Process Mapping of Cooling Rates and Thermal Gradient," PCT/US2013/055422, filed August 16, 2013.
  32. Fox, J.C. and Beuth, J.L., "Process Mapping of Transient Melt Pool Response in Wire Feed E-Beam Additive Manufacturing of Ti-6Al-4V," *Solid Freeform Fabrication Proceedings*, Austin, August 2013 (in the current proceedings).
  33. Beuth, J.L., and Fox, J.C., "Process Mapping of Thermal Response Due to Process Variable Changes," filed March 15, 2013.